NAVAL AIR WARFARE CENTER AIRCRAFT DIVISION
PATUXENT RIVER, MARYLAND

TECHNICAL INFORMATION MEMORANDUM

REPORT NO: NAWCADPAX/TIM-2014/79

SEA-BASED AUTOMATED LAUNCH AND RECOVERY SYSTEM VIRTUAL TESTBED

by

Colin H. Wilkinson
David B. Findlay
Kenny Boothe, Coherent Technical Services, Inc.
Surjan Dogra, Coherent Technical Services, Inc.

2 December 2013

DEPARTMENT OF THE NAVY
NAVAL AIR WARFARE CENTER AIRCRAFT DIVISION
PATUXENT RIVER, MARYLAND

NAWCADPAX/TIM-2014/79
2 December 2013

SEA-BASED AUTOMATED LAUNCH AND RECOVERY SYSTEM VIRTUAL TESTBED

by

Colin H. Wilkinson
David B. Findlay
Kenny Boothe, Coherent Technical Services, Inc.
Surjan Dogra, Coherent Technical Services, Inc.

RELEASED BY:

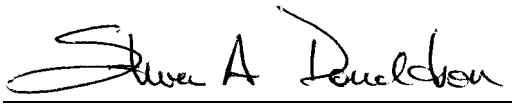

2 Dec 2013
STEVEN DONALDSON / AIR-4.3.2 / DATE
Head, Aeromechanics Division
Naval Air Warfare Center Aircraft Division

REPORT DOCUMENTATION PAGE

Form Approved
OMB No. 0704-0188

1. REPORT DATE	2. REPORT TYPE	3. DATES COVERED
2 December 2013	Technical Memorandum	

4. TITLE AND SUBTITLE	5a. CONTRACT NUMBER
Sea-Based Automated Launch and Recovery System Virtual Testbed	5b. GRANT NUMBER
	5c. PROGRAM ELEMENT NUMBER

6. AUTHOR(S)	5d. PROJECT NUMBER
Colin H. Wilkinson David B. Findlay Kenny Boothe, Coherent Technical Services, Inc. Surjan Dogra, Coherent Technical Services, Inc.	5e. TASK NUMBER
	5f. WORK UNIT NUMBER

7. PERFORMING ORGANIZATION NAME(S) AND ADDRESS(ES)	8. PERFORMING ORGANIZATION REPORT NUMBER
Naval Air Warfare Center Aircraft Division Bldg. 2187 48110 Shaw Road Patuxent River, MD 20670	NAWCADPAX/TIM-2014/79

9. SPONSORING/MONITORING AGENCY NAME(S) AND ADDRESS(ES)	10. SPONSOR/MONITOR'S ACRONYM(S)
Office of Naval Research Code 53 One Liberty Center 875 N. Randolph Street, Suite 1425 Arlington, VA 22203-1995	11. SPONSOR/MONITOR'S REPORT NUMBER(S)

12. DISTRIBUTION/AVAILABILITY STATEMENT

Approved for public release; distribution is unlimited.

13. SUPPLEMENTARY NOTES

14. ABSTRACT

The primary objective of the Sea-based Automated Launch and Recovery System (SALRS) program is to enable automated launch and recovery capabilities for sea-based naval aircraft. In support of this objective, the program is exploring the performance of sensors in degraded environments as well as the fusion of data from multiple sensors with Global Positioning System (GPS)/Inertial Navigation System (INS) technology. A simulation capability, the SALRS Virtual Testbed, is being built to facilitate testing of the technologies developed through SALRS in a high fidelity shipboard environment. The components and functionality of the testbed are described. A generic sensor model is used to simulate the effects of noise, dropouts and bias on the navigation signal, and the performance of a helicopter landing on a ship in degraded conditions is evaluated. Multiple sensor types are integrated with an Extended Kalman Filter to study sensor fusion in a fixed wing aircraft shipboard recovery scenario.

15. SUBJECT TERMS

Sea-Based Automated Launch and Recovery System (SALRS); Office of Naval Research (ONR); Virtual Testbed

16. SECURITY CLASSIFICATION OF:			17. LIMITATION OF ABSTRACT	18. NUMBER OF PAGES	19a. NAME OF RESPONSIBLE PERSON
a. REPORT	b. ABSTRACT	c. THIS PAGE			Colin Wilkinson
Unclassified	Unclassified	Unclassified	SAR	22	19b. TELEPHONE NUMBER (include area code) 301-342-9016

Standard Form 298 (Rev. 8-98)
Prescribed by ANSI Std. Z39-18

SUMMARY

The primary objective of the Sea-based Automated Launch and Recovery System (SALRS) program is to enable automated launch and recovery capabilities for sea-based naval aircraft. In support of this objective, the program is exploring the performance of sensors in degraded environments as well as the fusion of data from multiple sensors with Global Positioning System (GPS)/Inertial Navigation System (INS) technology. A simulation capability, the SALRS Virtual Testbed, is being built to facilitate testing of the technologies developed through SALRS in a high fidelity shipboard environment. The components and functionality of the testbed are described. A generic sensor model is used to simulate the effects of noise, dropouts and bias on the navigation signal, and the performance of a helicopter landing on a ship in degraded conditions is evaluated. Multiple sensor types are integrated with an Extended Kalman Filter to study sensor fusion in a fixed wing aircraft shipboard recovery scenario.

Contents

I. Introduction

The Office of Naval Research (ONR) sponsors a technology development program, titled Sea-based Autonomous Launch and Recovery System (SALRS), which seeks to develop technologies for precision relative navigation and guidance/control for an aircraft to perform automated or reduced pilot workload landings on air-capable ships. The vision of the SALRS program is to enable automated/semi-automated launch and recovery capabilities for sea-based naval aircraft, manned and unmanned, fixed wing and rotary wing, and to utilize automated or augmented pilot flight mechanics for carefree shipboard operations in the demanding Naval environment. This environment poses unique challenges due to deck motion, unsteady ship airwake, constrained space for safe operation, electromagnetic interference, severe weather, and degraded visual environments. SALRS is aimed at providing non-GPS-based options as a standalone capability, or to augment the Joint Precision Approach and Landing System (JPALS), which is GPS-based, for more robust autonomous guidance, navigation, and control (GNC) solutions. It employs workforce and infrastructure at NAVAIR and industry within the collaborative SALRS team. The initial approach is to analyze the requirements, perform top level trades to identify candidate sensors, model the most promising sensors, conduct virtual tests using high-fidelity simulations including modeling of sensors in degraded environments and deliver the resulting models and analysis to the user community. Future steps will update the models using real world test results, and use them to develop a system architecture and fusion capability.

The SALRS program was initiated in 2012. Through collaboration with industry, the program will explore the performance of sensors in degraded environments, including electro-optic/infra-red (EO/IR), radar, LIDAR/LADAR, beacon tracking and other novel approaches, as well as the fusion of data from multiple sensors with GPS/INS. The outcome will be increased efficiency, enhanced operational flexibility in the presence of extreme ship motion and degraded environmental conditions, and, through reduction in pilot landing workload, reduced cost of ship landing flight training.

This paper provides background on the requirement for SALRS, describes the SALRS Virtual Testbed simulation capability for shipboard autoland investigations, and presents the results of experiments with the testbed demonstrating the effects of degraded sensor data and fusion of multiple sensor configurations employing an Extended Kalman Filter (EKF) on automated shipboard recoveries. Performance of the sensors and filter performance are graded both on pure estimation error, and by examining the touchdown performance of the aircraft on the ship.

II. The SALRS Virtual Testbed

A key component of SALRS is the development of a Virtual Testbed with which to simulate all aspects of the shipboard environment relevant to aviation operations, including ocean, atmospheric and, ideally, electromagnetic conditions. The testbed will be used to evaluate the sensor and data fusion technologies developed through the SALRS program, and to demonstrate candidate autoland systems, as well as explore the operations aspects of automating shipboard launch and recovery.

The testbed, which is in the early stages of development, consists of a suite of desktop tools and piloted facilities, applicable to fixed and rotary wing aircraft, both manned and unmanned. The testbed builds on existing infrastructure and models, and benefits from considerable shipboard simulation experience gained at NAVAIR and throughout the simulation community in Government, academia and industry, nationally and internationally.

The Virtual Testbed is intended to be:

- Flexible & robust, to enable integration of multiple modes, sensors, configurations & scenarios
- Distributable to SALRS team members external to the Government
- Modular to ensure commonality and usability
- Selectable fidelity to enable fidelity levels appropriate for the application
- Desktop and piloted, to provide a range of analysis options

A. Virtual Testbed Environment

The SALRS Virtual Testbed is based on the Controls Analysis and Simulation Test Loop Environment (CASTLE®), developed by NAVAIR's Flight Vehicle Modeling and Simulation Branch[1,2]. CASTLE was created to provide rapid response to a wide range of Navy simulation requirements, evolving from the growing need to support an aircraft platform throughout its entire life cycle. In addition to supporting real-time high-fidelity pilot-in-the-loop simulations in the Navy's Manned Flight Simulator (MFS) facility, CASTLE includes integrated tools used for development and analysis of airframe simulations on various platforms, and hardware-in-the-loop (HIL) capability.

CASTLE has been linked with other simulation codes, including Matlab Simulink via an S-function allowing any Simulink model to be used with any CASTLE airframe model.

A CASTLE simulation consists of two executables, the CASTLE Graphical User Interface (GUI) and a user developed simulation executive, such as an airframe model (Figure 1). The GUI provides a means for the user to interact with the simulation executive. The simulation executive is the process that actually executes the calculations that represent the physical model being simulated. The GUI and simulation executive are physically separate processes that communicate via a message scheme over TCP/IP. Since a network protocol is used for inter-process communication, the GUI and the simulation executive need not run on the same computer. The GUI must run on a Microsoft Windows machine, but the simulation executive is platform-independent.

B. Components of the Virtual Testbed

The SALRS Virtual Testbed includes both desktop and piloted functionality. The desktop simulation is a PC-based offline simulation analysis program running in the CASTLE environment which enables an aircraft to be flown to a ship while experiencing realistic shipboard effects. The piloting task is taken care of by a pilot model. A full set of aircraft and environmental variables are recorded and can be processed using in-built CASTLE plotting and analysis functions or exported to Matlab. The desktop simulation supports multiple ship-aircraft combinations, including the F/A-18 aircraft model flying to a CVN aircraft carrier, and the in-house Example Helicopter (ExHel) model flying to a DDG destroyer or LHA amphibious class ship (Figure 2).

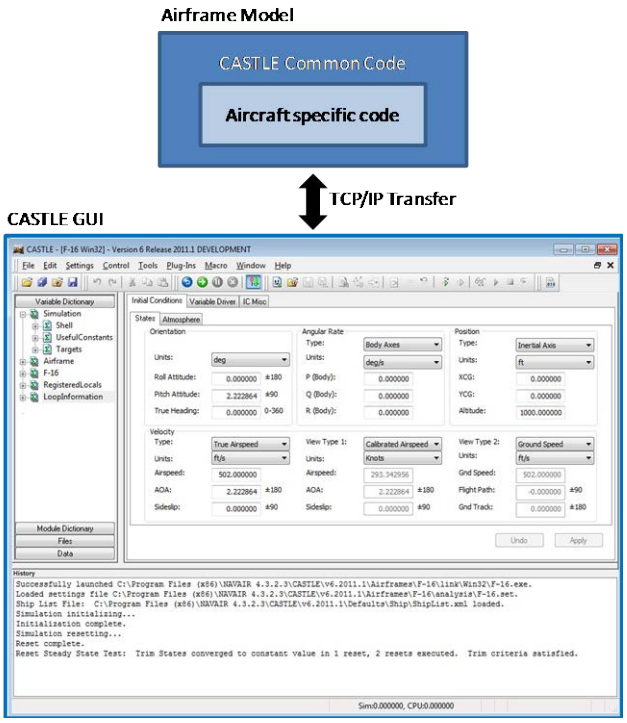

Figure 1. CASTLE Architecture.

The piloted component of the Virtual Testbed is also based on CASTLE, thereby easing the transition between offline and manned simulation, and encouraging model re-use. The piloted simulation makes use of the extensive flight simulation facilities at the MFS, which have been applied many times previously to shipboard operations. A range of aircraft specific and generic cockpits are available, for fixed wing and rotary wing aircraft, and can be operated in a fixed-base configuration or installed on the six degree-of-freedom (DOF) motion platform. Visual displays are provided by an Aechelon Technology pC Nova image generator, which includes a library of environment and weather effects, such as dusk horizon glow, real time shadows, haze, fog, lightning, rain and snow. Effects for forward looking infrared (FLIR), night vision devices (NVD) and radar are supported, and include automatic and manual gain control, noise, halos, bloom, and atmospherics.

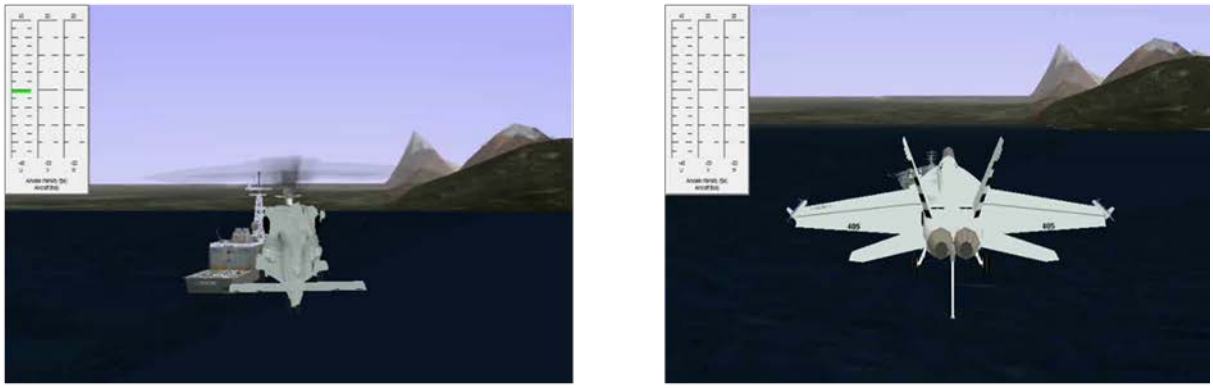

Figure 2. Desktop Simulation Rotary Wing Approach to DDG and Fixed Wing Approach to CVN.

The ExHel rotary wing simulation model was derived by NAVAIR from public source information and based primarily on Howlett[3]. This report is often referred to as the "GENHEL Math Model" and describes the main and tail rotor parameters, fuselage and empennage aerodynamics, flight control system, and basic mass properties. The engine model is derived from Ballin[4]. The main rotor is implemented as a blade element model using the data from the math model report, and the tail rotor can be selected as either a Bailey disc model or a blade element model. Landing gear characteristics are based on drawings and generalized oleo characteristics. Provisions are also made to connect the ExHel simulation to the piloted cockpit environment.

A controller was developed for ExHel to fly recoveries to ship flight decks. The controller has two parts. The inner portion is the pilot model and allows basic tracking of states such as altitude, heading and airspeed. It also includes longitudinal and lateral speed holds and position holds. This inner portion generates pilot inputs to the cyclic, collective and pedals. The outer portion, referred to as the task model, generates a set of commands for the pilot model based on the relative position of the aircraft to the desired landing spot. The task model commands the aircraft to approach the ship from a desired heading and descend along a desired glideslope. The approach profile is based on a typical visual approach to a DDG destroyer class ship starting 1.2 nm aft of the ship at 400 ft radar altitude and 80 kt airspeed. At 0.5 nm from the ship, the pilot model transitions to controlling closure rate with a desired closure between 15 and 20 kt. The last check point is 125 ft radar altitude when 0.25 nm from the ship which provides a 3 deg glideslope to a hover level with the top of the hangar. Once the aircraft is over the landing spot, the task model can optionally command a pedal turn to align with the ship. The pilot model then maintains position over the desired spot and finally lands on the deck by lowering the collective. The sequence of command modes used and the transition points between them is listed in Table 1.

Table 1. Pilot Model Command Sequence.

Phase	Mode	Transition to Next Phase
1	Airspeed Command Mode	Ground speed command close to desired ground speed
2	Ground Speed Command Mode (high-speed) Cross-track error controlled by heading Heading controlled by bank angle	Airspeed less than 35 kt
3	Ground speed Command Mode (low-speed) Cross-track error by lateral ground speed Current heading captured and held	Ground speed command from deceleration model equal to command from position mode.
4	Position Command Mode Heading held	Inside 20 ft of the landing spot
5	Position Command Mode, Pedal Turn Heading aligned with ship heading if pedal turn enabled	Within 5 ft radial of the landing spot with hysteresis
6	Hover hold	After 5 sec wait
7	Landing; lower collective lever	

The F/A-18 fixed wing aircraft simulation model covers most of the flight envelope for the aircraft. The model was developed primarily from wind-tunnel test data, with extensive flight test corrections. Full-envelope coverage is provided, with incremental surface deflection and store loading effects. The model is implemented using table lookups for the baseline and incremental effects, with linear interpolation between table breakpoints. Multiple

controllers are available to automatically fly the aircraft model to the ship, including the Automatic Carrier Landing System (ACLS) currently in operational use by the fleet, and a research controller which employs flight path rate command and flight path command to provide precision control during the carrier approach and landing phase.

The simulated ship models in the Virtual Testbed are driven in six degrees-of-freedom (pitch, roll, yaw, surge, sway and heave) via the Ship Motion Program/Ship Time History (SMP/STH) suite of models developed by the Naval Surface Warfare Center Carderock Division (NSWCCD)[5]. Models are available for all the major air-capable ship classes in the US Navy fleet and respond to changes in wave direction, significant wave height and modal period. The Virtual Testbed also includes a database of high fidelity, time accurate airwake models for multiple ship classes (Figure 3). The models were developed by NAVAIR using computational fluid dynamics (CFD), and have been integrated in the fixed wing and rotary wing simulations[6-9]. The airwake data are pre-computed and stored in a lookup-table as time histories of three-dimensional velocities on a grid surrounding the ship. Separate datasets exist for individual relative wind azimuths and the airwake velocities are scaled by relative wind speed. The airwake data are sampled by the ExHel blade element rotor model at each blade segment as well as locations on the fuselage and empennage, creating representative aircraft response and pilot workload to gusts in the vicinity of the ship. In the fixed wing simulations, the airwake is sampled at the center of gravity, and at the wingtips, nose and tail. The velocities applied to the CG directly affect the u, v, and w body-axis velocity components of the aircraft, while the velocities applied to the extremities are used to calculate estimated rotational components.

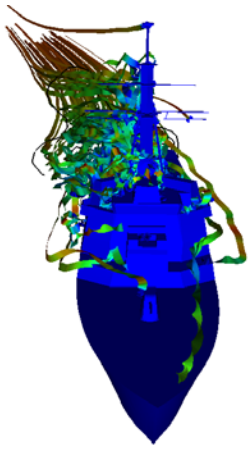

Figure 3. Representation of CFD Airwake over a DDG Class Ship.

As originally configured, the rotary wing and fixed wing controllers were provided with perfect ship-aircraft relative position data, which is clearly unrealistic in the real world. Noise, jamming, denial of service and other electromagnetic interference effects, both benign and hostile, must be accounted for, in addition to the limitations of communication between ship and aircraft where applicable. The fidelity to which these effects are modeled will form part of the multi-fidelity characteristics of the Virtual Testbed. For some applications, an effects-based model of the ship-relative navigation signal will be sufficient. For other applications, it will be necessary to interface with a physical model of the sensor, or suite of sensors, and in some cases with the actual sensor hardware, for which runtime control, handshaking protocols and latency issues will need to be addressed. As a starting point for representing the effects of sensed navigation data, a “generic sensor” model was created which introduces errors to the ship-relative navigation signal. The Virtual Testbed was used to evaluate the effects of these errors on the ability of the aircraft to recover to the ship. The generic sensor model, and the results of testing, will be described later in the paper.

The modular architecture of the testbed is configured to facilitate the insertion of additional ship and aircraft models. For example, a model of the US Navy Fire Scout UAV is currently being developed for incorporation in the tool. New ship airwakes, computed for either additional relative wind azimuths or additional ships, can also be added. The CASTLE GUI, which is common to both fixed wing and rotary wing applications, is used to control the simulation, and allows the user to execute single approaches or multiple approaches in batch mode. The desktop simulation, including the CASTLE environment, is releasable to contractors, with restrictions on some constituent models, for example the F/A-18E/F airframe. However, a generic fixed wing air vehicle model, termed Example Jet (ExJet), has also been developed to facilitate distribution to external agencies.

C. Virtual Testbed Development

The first phase of the SALRS Virtual Testbed development was completed in December 2012. The objective of Phase 1 was to demonstrate the potential of the existing NAVAIR shipboard simulation capability and use it to walk through the integration of an autoland simulation. The Phase 1 simulation included the generic aircraft models, ExHel and ExJet, as well as ship motion and airwake models to provide a representative shipboard environment. The sensor component was the generic sensor which modulated the relative ship-aircraft position vector based on rudimentary algorithms. The generic sensor was implemented as a temporary surrogate for a physics-based sensor to enable sensitivity analyses of landing performance in response to degraded environmental conditions. The outputs of the generic sensor can be tailored to represent a particular sensor type, examples of which are listed in Table 2. Interference effects were applied to the generic sensor output signal including bias, noise and sample-and-hold. The Phase 1 simulation addressed the effects of degraded environments on aircraft performance and explored how data

fusion might be effectively utilized to enhance performance over use of a single sensor. The results of these investigations will be described later in the paper.

Table 2. Generic Sensor Categories.

	Range	Azimuth Angle	Elevation Angle	Relative Altitude	Ranges to External Points of Reference	Relative Position	Relative Velocity
Global Positioning System					x	x	x
EOGRS[1]		x	x				
Tracking Radar	x	x	x				
Bedford Array[2]			x				
Barometric Altimeter				x			
LIDAR	x						
TACAN[3]	x	x					
IFLOLS[4]		x	x				
Image Sensor	x	x	x			x	

Notes:
1. EOGRS: Electro-Optical Grid Reference System (General Electric Aviation).
2. Bedford Array: provides glideslope information to pilots in the terminal phase of landing on an aircraft carrier.
3. TACAN: Tactical Airborne Navigation.
4. IFLOLS: Improved Fresnel Lens Optical Landing System. Provides glideslope information to pilots in the terminal phase of landing on an aircraft carrier.

Phase 2 is extending the Virtual Testbed to include specific sensors and aircraft models, both fixed wing and rotary wing, and will include a GPS/INS component to address integration with current on-board Precision Ship-Relative Navigation (PS-RN) technology, such as JPALS. Comparisons against flight test data will be an important component of the simulation development. The simulation will be used to evaluate the performance of sensors in perfect and degraded conditions, sensor fusion techniques for the shipboard task, and procedural issues associated with shipboard autoland. The simulation will be initially based on the ExJet fixed wing vehicle model and will subsequently include a platform representative of the Navy's future Unmanned Carrier Launched Airborne Surveillance and Strike (UCLASS) air vehicle. The rotary wing simulation will start with the generic ExHel helicopter and will transition to a Fire Scout model. The simulation will in general be non-real-time but the framework will be designed such that extension to real-time man-in-the-loop simulation is possible to explore the application of autoland technology to pilot augmentation. The architecture of the testbed is shown in Figure 4.

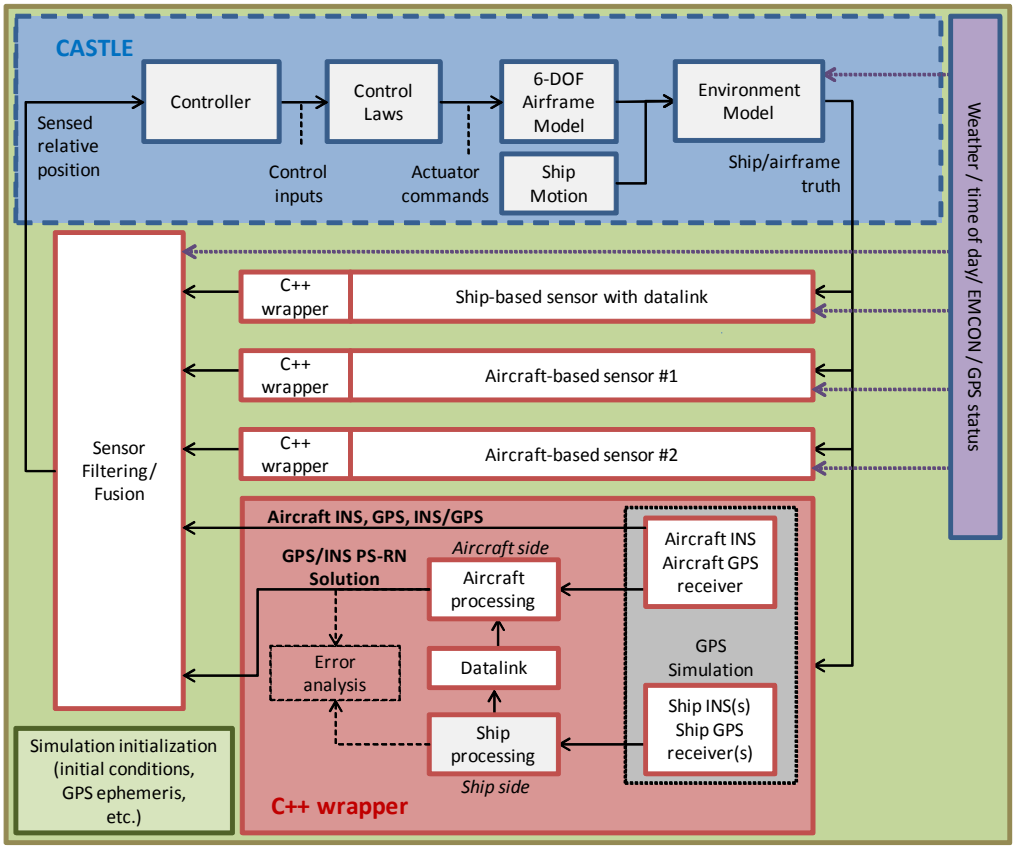

Figure 4. SALRS Simulation Architecture.

The simulation framework is being designed to enable future integration of higher fidelity physics-based sensors and sensor filtering/fusion techniques from multiple vendors as they become available through the SALRS program. To facilitate this capability, contractors are being requested to conform their models and algorithms to a common sensor model interface. A schematic of the interface is shown in Figure 5. The model interface will be created by the model provider, while the model wrapper/executive will be written by the Virtual Testbed team.

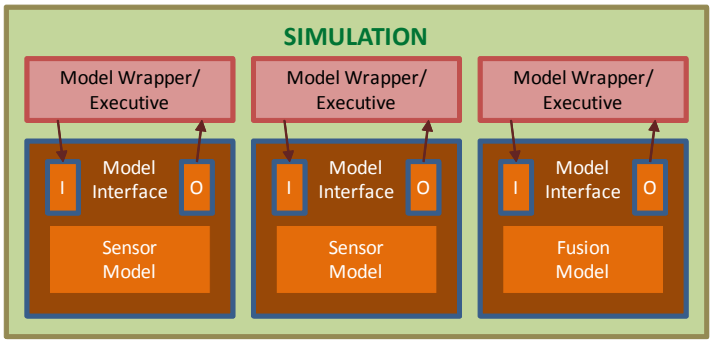

Figure 5. SALRS Common Interface.

III. Evaluation of Degraded Conditions on Rotary Wing Automated Landing

To evaluate the effects of degraded environmental conditions on helicopter performance for an automated recovery, the Virtual Testbed was configured to fly the ExHel vehicle model to a simulated DDG-81 destroyer, using the pilot model controller to approach the ship and land on the deck. For this simulation, the approach path was initiated 0.5 miles aft of the ship on a 3 deg glideslope for a straight-in approach, i.e. from 180 deg relative to the ship's head. Conditions for the baseline case were as follows:

- ship stationary in the water
- 25 kt of ambient wind from ahead
- zero airwake perturbations
- zero rotational or translational ship motion
- perfect ship-relative navigation signal, i.e. zero navigation sensor error (NSE)

The following analysis demonstrates the effect of adding airwake perturbations and ship motion to the simulation, and degrading the relative position information provided to the pilot model by introducing noise, dropouts and bias to the signal. The degradation levels are arbitrary and are not intended to represent any particular sensor or environmental condition. In general, data are plotted starting 20 s into the simulation, and ending at touchdown which is at approximately 80 s. It should be noted that the pilot model does not enforce a perfect track to the flight deck, even in the baseline case, but deviates in lateral track by up to 4 ft from the ideal due to cross-coupling effects in the controls and transients stemming from control mode transitions.

A. Effect of Airwake

Lateral cyclic position is plotted against time in Figure 6, comparing how the pilot model responds to the presence of gusts relative to the baseline case. The additional control activity required to maintain the desired track and hover is clearly visible. For a piloted aircraft, this would equate to additional workload. For an unmanned aircraft, the additional cyclic excursions may reduce available control margins or exceed the bandwidth of a real-world control system.

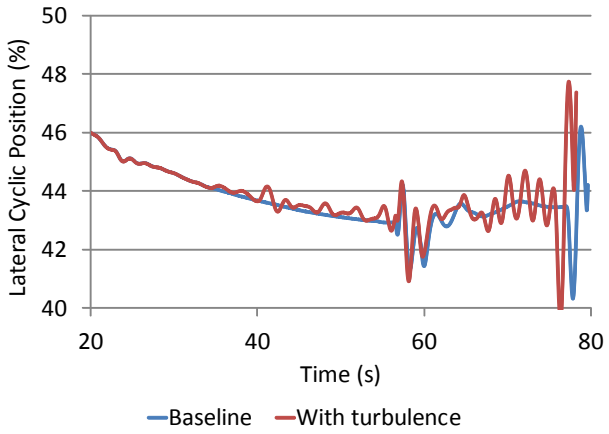

Figure 6. Effect of Airwake Perturbations on Lateral Cyclic Position.

B. Effect of Ship Motion

The effect of increasing levels of ship motion on the altitude of the aircraft as it approaches the ship is plotted in Figure 7. The ship motion levels are represented by sea states 4 (moderate), 5 (rough) and 6 (very rough). Only the final 30 s of data prior to touchdown are shown. The pilot model attempts to follow the motion of the flight deck and does not wait for a quiescent period before descending to the deck. This is in contrast to a real pilot who would typically establish a hover over the flight deck and let the ship move beneath him until the deck settles down. Nevertheless, if ship motion is high, the pilot will need to follow the ship, particularly in the final stages of landing to avoid unintentionally coming into contact with the deck.

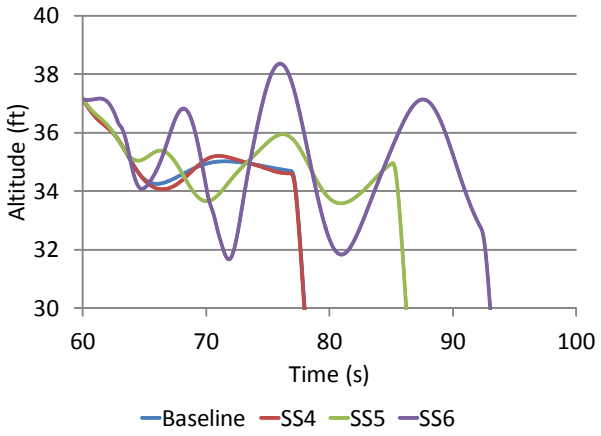

Figure 7. Effect of Ship Motion on Altitude.

C. Effect of Noise

Noise was added to the navigation signal through the generic sensor. The level of noise was constant throughout the approach and applied equally in each translational axis. Multiple simulation runs were conducted with noise levels of increasing standard deviation applied for each run. The NSE in the crosstrack axis for each level of noise is shown in Figure 8. Zero noise was applied in the baseline case.

The effect of noise on the crosstrack of the aircraft is shown in Figure 9. The red line shows how the aircraft responds when the Level 3 noise is added to the sensor signal. The black line is the actual aircraft position, and the purple line is the noisy position that the generic sensor is reporting to the pilot model. While the amplitude of noise is relatively small, the pilot model responds with deviations of up to 40 ft. The deviations are considerably damped when the model transitions from ground speed command mode to position command mode within 20 ft of the spot, which occurs at 65 s.

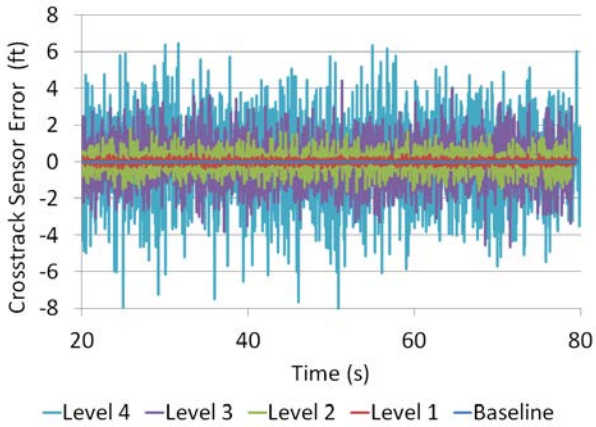

Figure 8. NSE due to Noise.

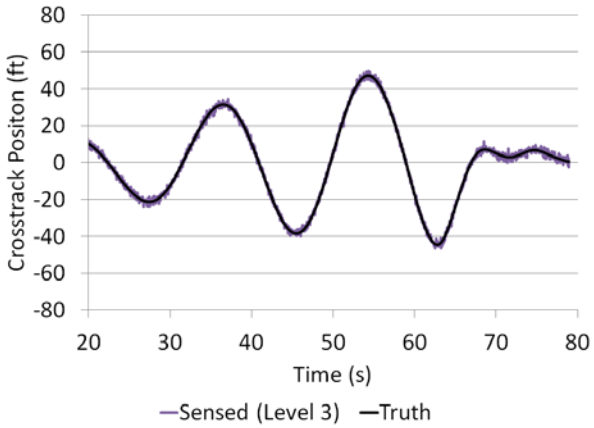

Figure 9. Effect of Noise on Crosstrack Position (Level 3).

The crosstrack position of the aircraft in response to the noise levels shown in Figure 8 are plotted in Figure 10. The amplitudes of the deviations from the ideal track are much increased between Levels 2 and 3.

Finally, the effect of noise on the Total System Error (TSE) is examined. The aircraft has an inherent amount of Flight Technical Error (FTE) and this is combined with NSE to yield the TSE, i.e.

$$TSE = NSE + FTE \tag{1}$$

In this case, the TSE metric of interest is the radial distance to the landing spot at touchdown (Figure 11). There is little impact on landing accuracy for noise levels up to Level 3, with all landings inside 1.5 ft of the spot. However, at Level 4, accuracy degrades to over 7 ft from the spot, which would typically be unacceptable for helicopter operations on small deck ships. These results are based on single events and a greater number of events should be sampled to draw firmer conclusions.

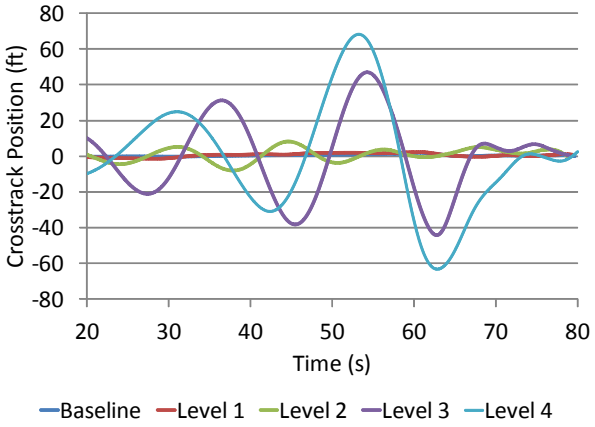

Figure 10. Effect of Noise on Crosstrack Position (All Levels).

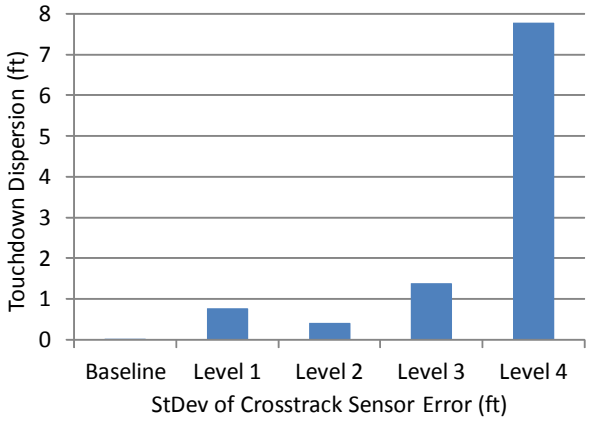

Figure 11. Effect of Noise on Distance to Spot at Touchdown (All Levels).

In the cases shown, the noise level is constant throughout the approach, which may or may not be realistic. Depending on the sensor and the conditions, the noise may decrease with decreasing range. Furthermore, the pilot model gains are not tuned for this scenario. A more intelligent model might react less aggressively at greater range to avoid the exaggerated overshoots seen here. Nevertheless, the results serve to indicate the potential effects of sensors in degraded environments and how the simulation might be used to evaluate these effects.

D. Effect of Dropouts

Dropouts in relative navigation information were modeled by the generic sensor with increasing periods and at random times as shown in Figure 12. Dropouts were applied simultaneously across all translational axes. The figure shows the NSE, i.e. the difference between the truth crosstrack position and the sensed position, for each level of

dropout severity. When no dropout is occurring, the NSE is zero. When a dropout occurs, the sensor outputs the last known position. However, the pilot model is not aware that the signal has failed. Thus, during a dropout, the pilot model either attempts to correct the sensed deviation from track with no apparent effect, requiring ever increasing control deflections, or maintains the current control inputs believing the aircraft to be on the correct trajectory. This continues until truth data is again restored at the end of the dropout, at which point the pilot model injects a restoring cyclic input. This process and its effect on crosstrack position are plotted in Figure 13 for the Level 4 case.

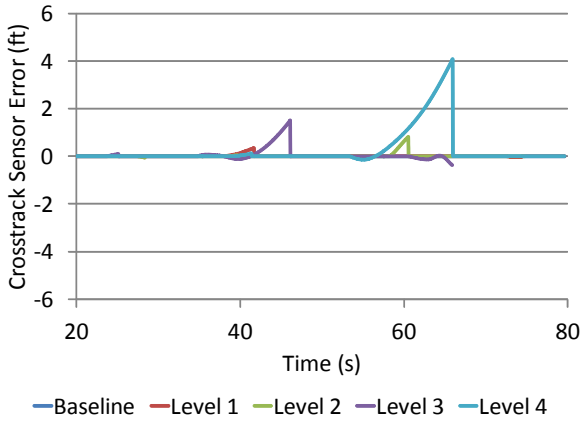

Figure 12. NSE due to Dropouts.

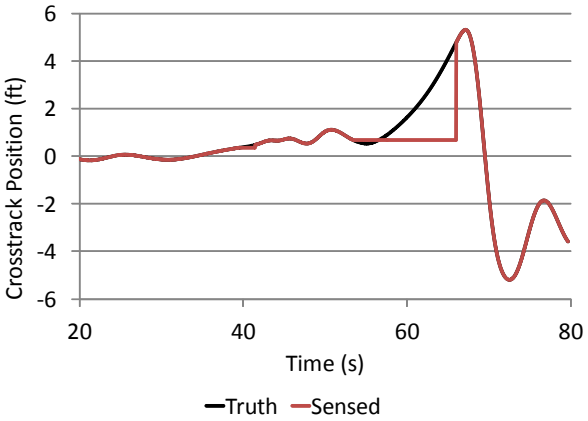

Figure 13. Effect of Dropouts on Crosstrack Position (Level 4).

The effect of all the dropout levels on crosstrack position is shown in Figure 14. For Level 4, a long dropout occurred close to the ship, resulting in the pilot model overcorrecting at the end of the dropout to such an extent that the aircraft lost track of the deck and failed to land. This is a potential real world situation if the ship disappears from the aircraft-mounted sensor's field-of-view or, equally, if the aircraft moves outside a ship-mounted sensor's field-of-view.

The radial distance to the landing spot at touchdown is plotted in Figure 15 for each of the dropout levels of severity. The bar for Level 4 is missing because the aircraft failed to land. The landing scatter for Levels 1 and 2 is within 1 ft. In these runs, the dropouts were either so short or occurred sufficiently distant from the ship that the pilot model was able to correct the track and execute a landing as if nothing had happened. The dropouts have a more significant effect at Level 3 where the aircraft lands almost 3 ft from the spot.

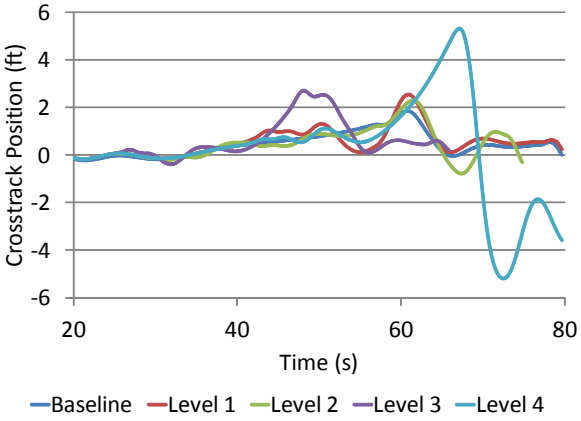

Figure 14. Effect of Dropouts on Crosstrack Position (All Levels).

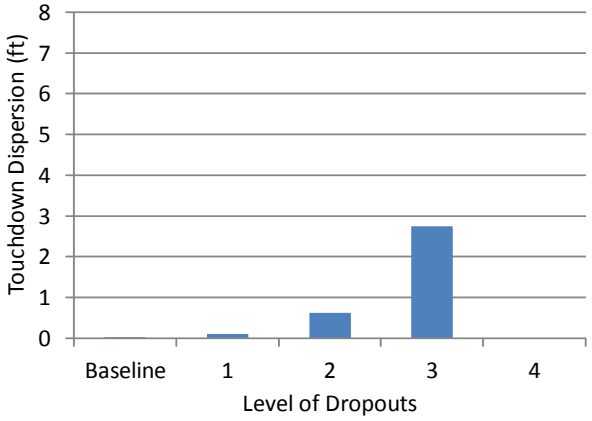

Figure 15. Effect of Dropouts on Distance to Spot at Touchdown (All Levels).

E. Effect of Bias

A range of biases were applied to the relative position data generated by the generic sensor. The biases were equally applied in each translational axis. The biases on the crosstrack sensor signal are shown in Figure 16. The bias was constant until the aircraft was 1000 ft from the ship, and then decreased linearly with distance.

The effect on crosstrack position of each level of bias is plotted in Figure 17. The response of the aircraft is consistent across each level.

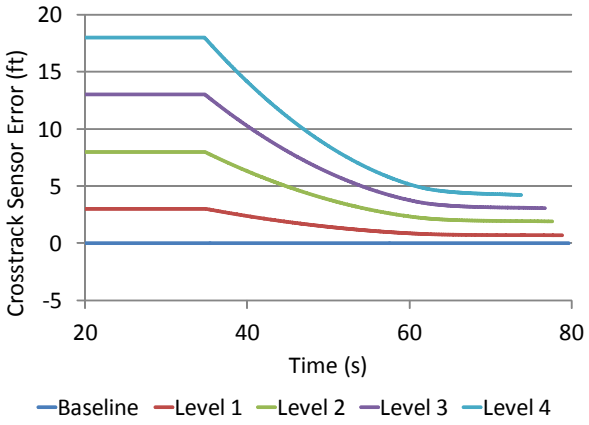

Figure 16. NSE due to Bias.

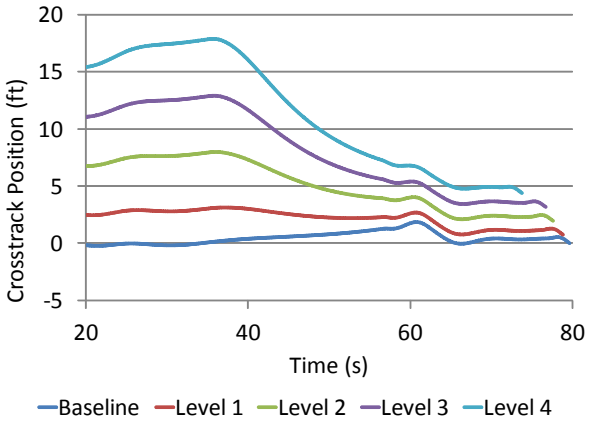

Figure 17. Effect of Bias on Crosstrack Position (All Levels).

The effect of each bias level on touchdown performance is plotted in Figure 18. The increasing bias in the position information results in the aircraft landing further from the landing spot. In fact, the aircraft will attempt to land no matter how large the bias, because it thinks it is over the spot based on the sensed relative position.

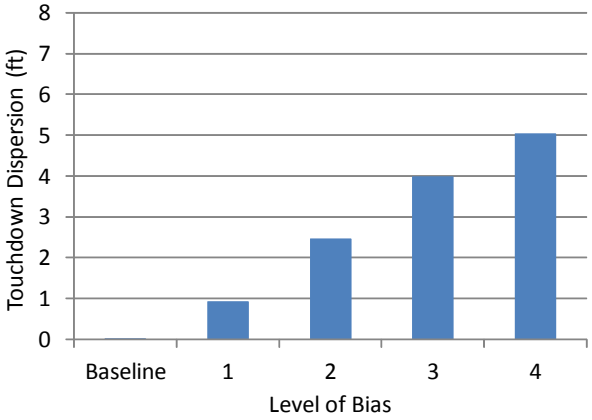

Figure 18. Effect of Bias on Distance to Spot at Touchdown (All Levels).

IV. Evaluation of EKF Performance for Fixed Wing Automated Landing

A Matlab® version of the SALRS Virtual Testbed was created by Coherent Technical Services, Inc. (CTSi) to facilitate GNC algorithm development. Matlab provides a familiar interface to engineers who may not be adept at working in the C++ environment of the testbed, and leaves the many pre-existing Matlab functions and toolboxes at their disposal. This simulation environment includes all the major components from Figure 4 and uses CASTLE aircraft and ship models. Utilizing CASTLE through its provided Simulink interface, the initial conditions can be varied to perform batch mode Monte Carlo analysis of multiple configurations in a statistically meaningful way.

This version of the testbed was used to investigate the use of an EKF with various sensor configurations applied to a fixed wing air vehicle conducting automated approaches to an aircraft carrier. In the simulation, relative positioning sensors were added to the state feedback coming from the aircraft bus data, as if such sensors were installed on the aircraft. CASTLE provided all of the necessary states as outputs, taking control positions as inputs to close the loop. Four combinations of three sensor types from Table 2 were configured as inputs to the EKF.

The chief goal of this study was to test the performance of an EKF in the presence of representative sensor models. Placing the sensor models in the loop with data produced from a carrier landing simulation such as this assures that the impacts of dynamic and kinematic interactions between the aircraft and the ship motion are adequately captured. This leads to a secondary level of analysis, which is the evaluation of the total system performance, to include both the EKF and the automatic landing control system. The sensor model and EKF designs are described in the next section. Landing dispersion data are presented as the primary basis of comparison and the main topic of discussion.

A. EKF Formulation

The EKF used in this study takes the form of a typical GPS-aided INS. However, alternative position sensors are also used, in lieu of the GPS, as a calibrating mechanism for the INS. All positioning sensors operate at 2 Hz, while the inertial sensors provide measurements at 20 Hz. The EKF is designed to take multiple redundant relative positioning sensors as input, in concordance with the SALRS program goal of using the best available data at any given time. There are two basic concepts to integrate the relative inertial solution with multiple sensors:

1. Integration in the Position Domain (Figure 19)

Here measurements from multiple sensors are first converted into a relative position solution which is then integrated with the relative solution. The state estimator in this integration estimates the errors in the inertial solution, which are then used to calibrate the inertial solution.

2. Integration in the Measurement Domain (Figure 20).

In this configuration, measurements from multiple sensors are directly integrated with the relative solution. Again, the state estimator estimates the errors in the inertial solution, which are used to calibrate the inertial solution.

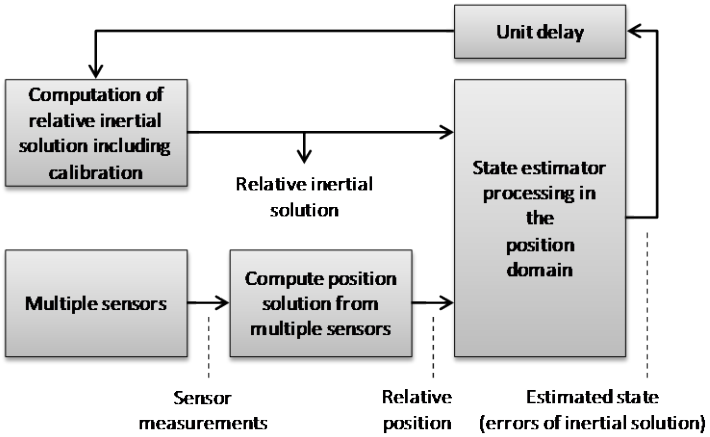

Figure 19. Position Domain Block Diagram.

Unless there is a compelling reason to integrate in the position domain, measurements should be integrated directly in the measurement domain of each sensor as each measurement has its own analytical link to the state being estimated. There are many benefits that result from integration in the measurement domain. One important benefit is to use whatever valid measurements are available at the measurement time, even if they don't lend themselves to first computing a position solution.

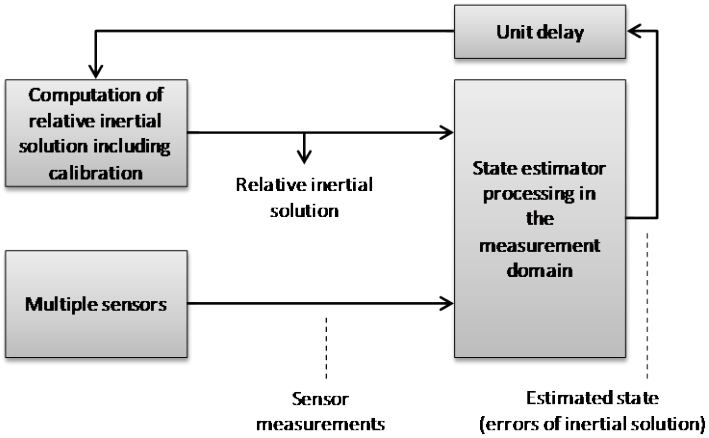

Figure 20. Measurement Domain Block Diagram.

Unless there is a compelling reason not to use some specific measurement, it is desirable to use fault free measurements from all available sensors. There is no need to screen measurements and use only those that come from the most accurate sensors. The state estimator is smart in the sense that it automatically weighs the measurements according to their statistical accuracy and produces the most statistically accurate solution.

A sensor fusion approach was developed that describes the integration of multiple sensors with the relative inertial solution between two moving platforms (Figure 21). The purpose of this integration is to calibrate the inertial solution and maintain its accuracy while navigating. The solution approach is to use measurements from all available sensors and integrate in the measurement domain of each sensor. The following types of sensors were considered in this study:

- Relative position sensor (e.g. GPS)
- Relative azimuth angle sensor
- Relative elevation angle sensor
- Relative range sensor

The EKF has been in use for solving integrated navigation problems ever since R.E. Kalman published his paper on filtering theory almost five decades ago. Even though the EKF is not optimal (only the Kalman Filter, which is based on linear system theory, is optimal), it has served estimation theory practitioners quite well. We have initially

developed the estimation equations based on the EKF. Noisy measurements come from sensors and predicted measurements are computed based on the relative inertial solution (which might have slowly changing errors in it). Sensor measurements and predicted measurements, together with their associated covariance matrices, are presented to the EKF, which estimates the errors in the relative inertial solution. These estimated errors are then used to correct the relative inertial solution. The process repeats at all subsequent time instants. In between sensor measurements, the inertial solution simply propagates using the most recent estimated errors.

The three classes of sensors used in this study are listed in Table 3. In order to investigate the practice of blending disparate sensor types with separate measurement domains, four separate sensor configurations were formed. These are summarized in Table 4, and describe the inputs to the EKF.

The guidance algorithms used for the simulation regulated crosstrack and altitude errors by producing altitude rate and heading angle commands. The system was designed to be compatible with the existing ACLS so that the guidance and control laws can be interchanged as needed.

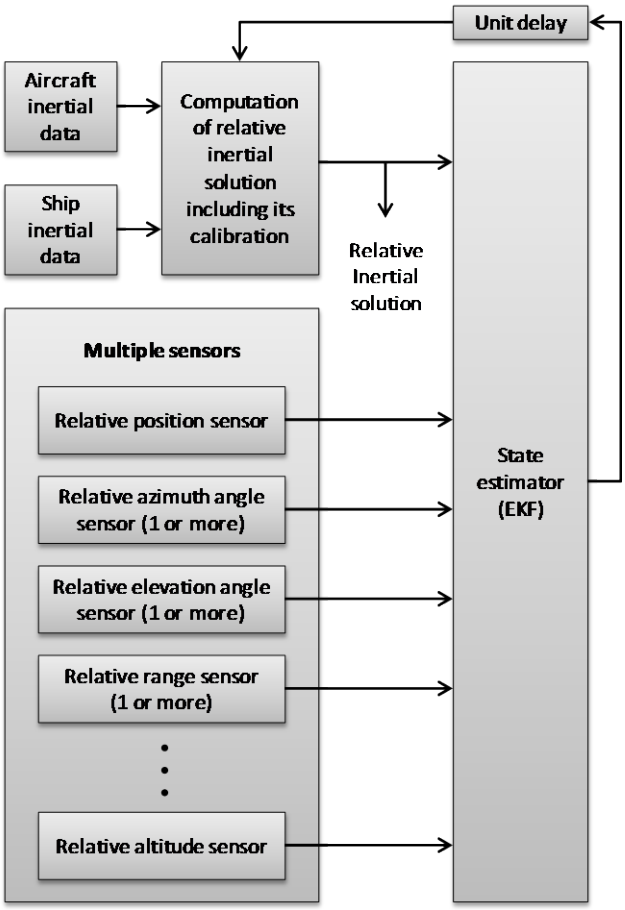

Figure 21. State Estimation Block Diagram.

B. Simulation Results

A Monte Carlo simulation was performed in which the initial position and orientation of the aircraft were varied across a bounded set. No airwake turbulence was included but the ship motion model added a pseudo random element into the results. The aircraft was positioned 6 nm aft of the ship at an altitude of 1200 ft. The Monte Carlo assignments made during initialization introduced variances in the initial heading and cross track error. The aircraft then proceeded with a typical approach, with the tip-over to glideslope occurring approximately 3.5 nm from the ship, as driven by the nominal 3.5 deg glideslope angle.

First, the NSE across the four filter configurations is examined (Figure 22). This is the total relative positional error between the truth and the estimate from the EKF. Performance across the configurations varies at longer ranges, but all solutions converge to an error of less than 2 ft as the aircraft nears the touchdown point (TDP). This is due to the fact that the attitude errors have less of an impact on the position estimates as the lever arm on the angular sensors decreases. The REL AZ EL M2 has a particularly low level of performance at range. One may expect this as the position is estimated solely from AZ/EL sensors, and suffers from the confluence of multiple attitude error effects, without the aid of a ranging sensor.

Table 3. Sensor Types.

Name	Type	Abbreviation
GPS	Relative position derived from absolute positions of ship and aircraft	POS
EOGRS	Azimuth / elevation	AZ EL
LIDAR	Range	RAN

Table 4. Sensor Configurations.

Configuration	Abbreviation
GPS only (baseline)	REL POS
Single EOGRS, single LIDAR	REL AZ EL RAN
Dual EOGRS	REL AZ EL M2[1]
Dual EOGRS, single LIDAR	REL AZ EL M2[1] RAN

Note: 1. M2 = dual measurements

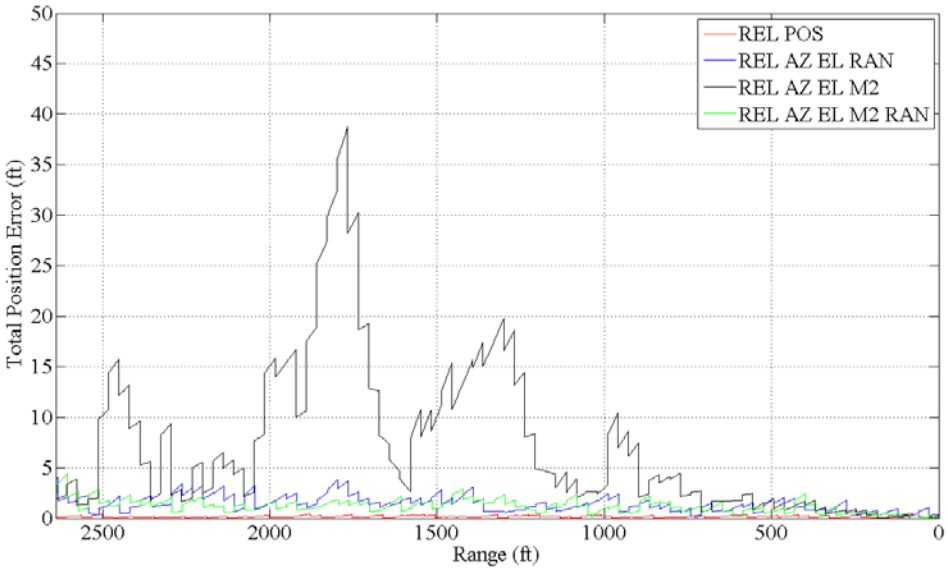

Figure 22. NSE vs. Range.

Next, the impact of the NSE on the TSE is examined. In this case, the TSE metric of interest is the total distance between the tailhook and the TDP when the tailhook crosses the wire axis, which is 0.75 ft above the deck. The TDP is located on the centerline of the runway, midway between the second and third arresting wires, as detailed in Figure 23.

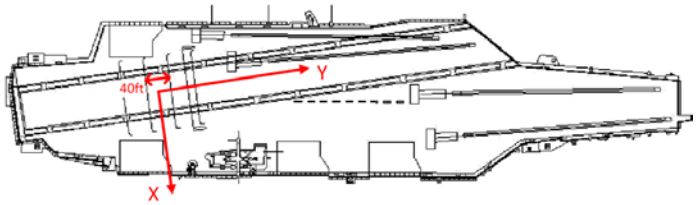

Figure 23. TDP Coordinate System.

Figure 24 shows the crosstrack error experienced by the aircraft across the four filter configurations. The performance of the REL POS configuration has no functional dependence on range and has the best performance throughout the run. The crosstrack error is driven to an acceptable level by the controller for all four configurations. The NSE causes excursions in TSE as the guidance system attempts to regulate these errors. However, the total system performance converges to an acceptable level near the TDP as the errors subside, and the control laws minimize the positional errors.

The Monte Carlo simulation consisted of 100 runs per sensor configuration. These 400 total runs took approximately 15 hours to complete. Figure 25 shows the touchdown scatter plots in the TDP coordinate system. Table 5 lists the mean and standard deviations for the total distance from the tailhook to the TDP. The results show that there is no clear advantage amongst the four sensor configurations. All of them, in conjunction with the EKF-based sensor-aided INS, provide the control system with a suitable estimate of the tailhook-to-TDP vector where it counts most – just prior to touchdown. All configurations catch the target third wire 100% of the time, and do so within a substantial margin. However, the introduction of airwake turbulence is expected to increase the TSE.

Table 5. TDP Dispersion Summary.

Sensor Configuration	Average total error at TDP (ft)	Standard deviation of total error at TDP (ft)
REL POS	2.8	2.0
REL AZ EL RAN	3.3	2.3
REL AZ EL M2	2.6	2.2
REL AZ EL M2 RAN	2.7	2.0

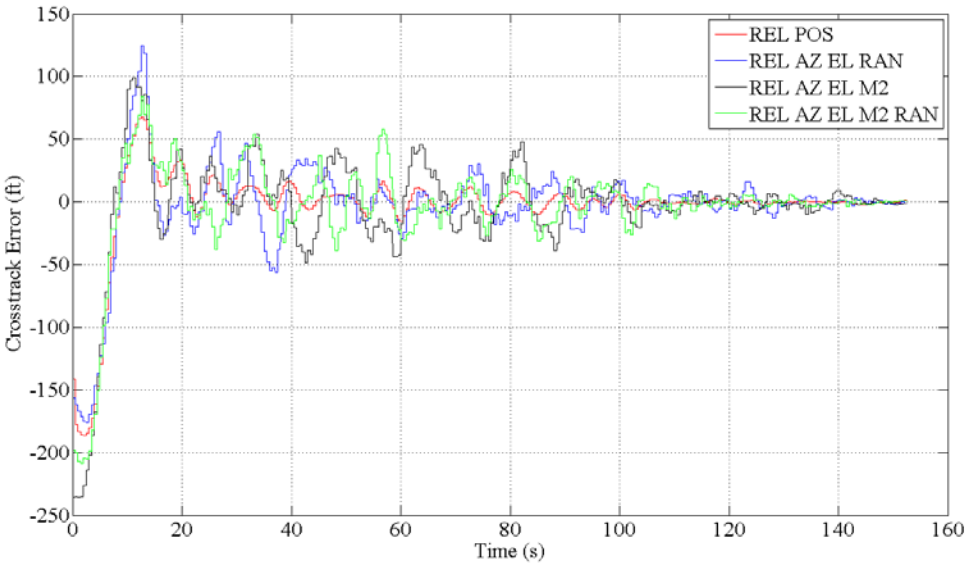

Figure 24. Crosstrack Position Error.

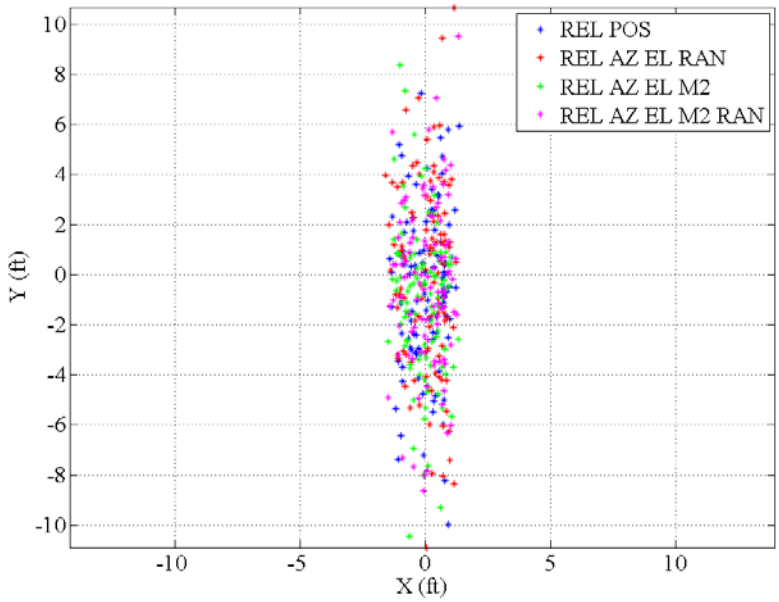

Figure 25. TDP Dispersions.

V. Conclusions

The SALRS Virtual Testbed was used to evaluate the impact of degraded environmental conditions on the landing performance of a helicopter flying to the flight deck of a DDG class destroyer in an automated closed-loop simulation. Airwake turbulence was shown to increase the control activity necessary to fly to the ship, while ship motion introduced deviations from the baseline approach path as the controller attempted to follow the moving flight deck. Navigation sensor errors were introduced in the form of noise, dropouts and bias to the relative position signal, and the effects on crosstrack position and touchdown dispersion were evaluated. Signal noise resulted in wide deviations from the baseline path, especially while the pilot model was operating in velocity command mode. Touchdown dispersions were within 1.5 ft of the landing spot for low NSE but rapidly increased to over 7 ft with higher NSE. Signal dropouts resulted in the aircraft losing track until the sensor signal was restored, and the aircraft failed to land when the dropout occurred in close proximity to the ship. Increasing levels of bias in the signal led to landings at increasing distances from the spot.

A Matlab version of the testbed was used to investigate the use of an EKF with various sensor configurations applied to a fixed wing air vehicle conducting automated approaches to an aircraft carrier. Sensor configurations included GPS only for the baseline case, as well as a LIDAR range sensor, and single and dual EOGRS systems providing azimuth and elevation. Within 250 ft of the ship, the NSE was within 2 ft across all sensor configurations. The crosstrack position error converged to acceptable values close to the ship, resulting in consistent capture of the target third wire in the absence of airwake turbulence.

These experiments demonstrate the utility of the SALRS Virtual Testbed for simulation evaluation of sensors in degraded environments and sensor fusion techniques. The testbed will be extended in the future to incorporate physics-based sensor models and more complex fusion algorithms via a common sensor interface.

References

1. York, B.W., Magyar, T.J., and Nichols, J.H., "Castle: The Next Generation of Navy Flight Simulation", *presented at the AIAA Modeling and Simulation Technologies Conference & Exhibit*, Montreal, Canada, 6-9 Aug, 2001. AlAA-2001-4243.
2. Magyar, T.J., and Page, A.P., "Integration of the CASTLE Simulation Executive with Simulink", *presented at the AIAA Modeling and Simulation Technologies Conference & Exhibit*, Montreal, Canada, 6-9 Aug, 2001. AIAA-2001-4121.
3. Howlett, J., "UH-60A Black Hawk Engineering Simulation Program: Volume I: Mathematical Model", NASA-CR-166309, Dec 1981.
4. Ballin, M., "A High Fidelity Real-Time Simulation of a Small Turboshaft Engine", NASA-TM-100991, Jul 1988.
5. Baltis, V.E., Applebee, T.R., and Meyers, W.G., "Validation of the Standard Ship Motion Program, SMP: Ship Motion Transfer Function Prediction", David W. Taylor Naval Ship Research and Development Center, Rept. DTNSRDC/SPD-0936-03, Jul 1981.
6. Polsky, S.A., and Bruner, C.W.S., "Time-Accurate Computational Simulations of an LHA Ship Airwake", *presented at the 18th AIAA Applied Aerodynamics Conference*, Denver, CO, 14-17 Aug, 2000. AIAA-2000-4126.
7. Polsky, S.A., "CFD Prediction of Airwake Flowfields for Ships Experiencing Beam Winds", presented at the *21st AIAA Applied Aerodynamics Conference*, Orlando, FL, 23-26 Jun 2003. AIAA-2003-3657.
8. Polsky, S., and Naylor, S., "CVN Airwake Modeling and Integration: Initial Steps in the Creation and Implementation of a Virtual Burble for F-18 Carrier Landing Simulations", *presented at the AIAA Modeling and Simulation Technologies Conference and Exhibit*, San Francisco, CA, 15-18 Aug 2005. AIAA-2005-6298.
9. Polsky, S., Imber, R., Czerwiec, R., and Ghee, T., "A Computational and Experimental Determination of the Air Flow around the Landing Deck of a US Navy Destroyer (DDG): Part II", *presented at the 37th AIAA Fluid Dynamics Conference and Exhibit*, Jun 2007. AIAA-2007-4484.

DISTRIBUTION:

NAVAIRWARCENACDIV (4.3.2.1/Wilkinson), Bldg. 2187 (2)
48110 Shaw Road, Patuxent River, MD 20670
NAVAIRWARCENACDIV (4.12.6.2), Bldg. 407, Room 116 (1)
22269 Cedar Point Road, Patuxent River, MD 20670-1120
DTIC (1)
8725 John J. Kingman Road, Suite 0944, Ft. Belvoir, VA 22060-6218